

Severe Hot Corrosion of the Superalloy IN718 in Mixed Salts of Na_2SO_4 and V_2O_5 at 700 °C

Dhananjay Pradhan, Girija Shankar Mahobia, Kausik Chattopadhyay, and Vakil Singh

(Submitted December 28, 2017; in revised form May 9, 2018; published online July 13, 2018)

This study presents hot corrosion behavior of the superalloy IN718 in 100 wt.% NaCl (salt S) and in salt mixtures of 60 wt.% Na_2SO_4 + 40 wt.% V_2O_5 (SM1) and 75 wt.% Na_2SO_4 + 15 wt.% NaCl + 10 wt.% V_2O_5 (SM2), deposited separately by spray gun technique, at elevated temperature of 700 °C. The weight gain per unit area at 700 °C was increased by 49% for salt S, 153% for the dual salt mixture SM1, and only 8% for the triple salt mixture SM2, in comparison with that observed earlier at 600 °C. The marked increase in the severity of corrosion at 700 °C is attributed to formation of the highly damaging compound NaVO_3 that significantly enhances the oxygen activity, in the SM1 coated samples. The effect of surface roughness and dislocation density on corrosion behavior at 700 °C, however, is found to be similar to that at 600 °C. Ultrasonic shot peening, a novel technique of surface modification, is found to enhance the hot corrosion resistance in the salt mixture SM1 at 700 °C appreciably due to extensive grain refinement to nanoscale and formation of highly protective Cr_2O_3 layer in the surface region.

Keywords corrosion kinetics, hot corrosion, salt and salt mixtures, ultrasonic shot peening

1. Introduction

Gas turbines operating in marine environment where ingestion of solid particles of NaCl is unavoidable, undergo severe corrosion at elevated temperature. Therefore, materials with high strength and high corrosion resistance are required for power generation and aero engine components in such environments. The Ni-Fe-based superalloy IN718 is mostly used as disk and blade material in compressor section of the gas turbine engines of advanced power plants and aero engines (Ref 1). Although Ni-base superalloys possess good strength at the operating temperatures of turbines, but suffer from hot corrosion from salts in the marine environment (Ref 2, 3). It is well known that in hot corrosion salt/salt mixtures fuse and accelerate the rate of oxidation and sulfidation of superalloys at elevated temperature. There are two types of hot corrosion; high-temperature hot corrosion (HTHC) above 750 °C, and low-temperature hot corrosion (LTHC) in the temperature range of 550-750 °C. In the HTHC, Na_2SO_4 undergoes melting, whereas in LTHC it forms eutectic of Na_2SO_4 - MSO_4 (M=Ni, Co, and Fe) (Ref 4-6). In the NaCl environment, corrosion rate is highly dependent on the oxygen partial pressure and corrosion rate is increased. The high rate of dissolution of such materials indicated that the protective oxides formed on them were not effective in the molten NaCl (Ref 5, 7). There was intense spalling, sputtering, and enormous weight gain during HTHC in aggressive environments (Ref 8-19). Electrochemical hot corrosion tests were performed in Na_2SO_4 ,

$80\text{V}_2\text{O}_5 + 20\text{Na}_2\text{SO}_4$, and NaVO_3 environments; corrosion rate was found to increase in the Na_2SO_4 and NaVO_3 with increase in temperature (Ref 20). Corrosion rate of the Cr/Co-Al coated superalloy was lower than that of the uncoated one due to formation of continuous, dense, adherent, and protective oxide scale over the surface of the component (Ref 21). The protective oxide scales were thin layers of Cr_2O_3 , Al_2O_3 , and CoCr_2O_4 which formed over the Cr/Co-Al coated superalloy substrate, exposed to the molten salt environment of Na_2SO_4 -60% V_2O_5 , at 900 °C. $(\text{Cr}(1-x)\text{Al}_x)\text{N}$ coatings with three different chemical compositions were deposited using magnetron sputtering of an industrial size PVD coater CC800/9, and significantly higher hot corrosion resistance was observed for the coated samples in the Na_2SO_4 environment in respect of the uncoated one. The excellent corrosion resistant behavior of the coated sample was attributed to formation of a protective scale on the coated surface, consisting of mainly a dense Al_2O_3 layer (Ref 22). Several investigations have been carried out related to hot corrosion in different salt mixtures for different protective coatings and TBCs (Ref 23, 24).

Thus, it may clearly be seen that due to the presence of salts like NaCl, Na_2SO_4 , and V_2O_5 , hot corrosion resistance of the superalloy IN718 is drastically reduced. In the case of marine gas turbines, filters are used to remove NaCl particles suspended in air; however, since volume of the air used is too large, NaCl particles invariably remain there in the ingested air. Sulfur and vanadium in the fuel form Na_2SO_4 and V_2O_5 compounds during combustion. Deposition of salts on surface of alloys leads to deterioration of the protective oxides. As the time passes, corrosion products penetrate the alloy by diffusion, corrode the substrate repeatedly, and roughen the surface. The problem of hot corrosion has drawn attention of researchers due to increase in the inlet temperature of gas turbines and lowering of chromium content of advanced superalloys (Ref 25-32). It is known that a surface with higher roughness is more prone to corrosion due to increase in the surface area (Ref 33). In our previous study, the effect of surface roughness was investigated on corrosion behavior of the superalloy IN718 in the salt S and in the salt mixtures SM1 and SM2, at 600 °C (Ref 34). The rate

Dhananjay Pradhan, Girija Shankar Mahobia, Kausik Chattopadhyay, and Vakil Singh, Department of Metallurgical Engineering, Indian Institute of Technology (Banaras Hindu University), Varanasi, India. Contact e-mail: dhananjay.rs.met13@iitbhu.ac.in.

of corrosion was found to increase with roughness of the surface and was highest in the salt S, followed by those in the salt mixtures SM2 and SM1.

Several means are being used to modify the surface and develop nanostructure. Ultrasonic shot peening is a relatively new process of generating surface nanostructure. Mechanical properties of metallic materials are significantly improved by surface nanostructuring without changing their chemical compositions (Ref 35, 36). Effect of surface grain refinement by shot peening was studied on oxidation behavior of the Inconel 800 alloy, and improvement in oxidation resistance was observed (Ref 37). Similar enhancement in oxidation resistance from surface nanostructuring has also been observed in zirconium (Ref 38). The effect of surface nanostructuring from ultrasonic shot peening was studied on hot corrosion behavior of Ti-6Al-4V, at 400, 500, and 600 °C, and the hot corrosion resistance was found to improve due to ultrasonic shot peening (Ref 39). However, there is no report on the effect of ultrasonic shot peening on hot corrosion behavior of the superalloy IN718.

The present work is an extension of our previous work at 600 °C on hot corrosion of the alloy IN718, to study the effect of the salt S, and salt mixtures SM1 and SM2, on the specimens of varying roughness, at higher temperature of 700 °C and to compare with that at 600 °C (Ref 34). In addition, the effect of ultrasonic shot peening is studied on hot corrosion resistance of this alloy in the salt mixture SM1 at 700 °C.

2. Experimental

The chemical composition, heat treatment cycle, sample preparation, surface roughness measurement, the process of salt coating, and the procedure of hot corrosion test of the superalloy IN718 used in the present investigation are reported in our earlier publication (Ref 34). In this study, dislocation density and microhardness of the specimens, of different surface roughness, were also evaluated using XRD and Leco microhardness tester, respectively. For surface modification, a novel technique of ultrasonic shot peening was used and this process is described in detail elsewhere (Ref 35). It is relevant

to mention that prior to USP treatment the sample was mechanically polished and its surface roughness was 0.08 μm. It was subjected to ultrasonic shot peening using Stress Voyager (SONATS) for 5 min with hardened steel balls of 3 mm diameter, at a frequency of 20 kHz, at constant amplitude of 80 μm, and the hot corrosion tests were conducted. The oxidized and corroded specimens were washed in hot distilled water and subsequently in acetone using ultrasonic cleaner for microscopic examination. Scanning electron microscopy (SEM) and x-ray diffraction study were carried out for analyzing the oxidation and corrosion products. The cross section morphology was examined by scanning electron microscope (Zeiss EVO/18). Also the cross section of the sample ground on 400 grit and hot corroded by the salt mixture SM1 was examined using the Electron Probe Micro Analyzer (EPMA) CAMECA SX Five instrument for the distribution of elements in the oxide layer and substrate.

3. Results

3.1 Dislocation Density and Microhardness

Dislocation density (ρ) of the samples ground with 1000 (R_{a1}), 800 (R_{a2}), 600 (R_{a3}), and 400 (R_{a4}) grit SiC emery papers was calculated by XRD and using the relationship given below (Ref 40):

$$\rho = \frac{3\sqrt{2}\pi}{Db} (\varepsilon^2)^{1/2} \quad (\text{Eq 1})$$

where D is average crystallite size [Scherrer and Wilson equation (Ref 41), $D = \frac{0.9\lambda}{B \cos \theta}$], ε is micro strain [Williamson Hall equation (Ref 42), $B \cos \theta = \frac{0.9\lambda}{D} + 4\varepsilon \sin \theta$, λ is x-ray wavelength, θ is Bragg angle, and B is line broadening], b is Burgers vector ($b = a/\sqrt{2}$ for FCC structure), and a is lattice parameter. The dislocation density corresponding to average roughness of R_{a1} , R_{a2} , R_{a3} , and R_{a4} was estimated to be $1.9 \times 10^9 \text{ m}^{-2}$ (ρ_1), $2.48 \times 10^9 \text{ m}^{-2}$ (ρ_2), $2.66 \times 10^9 \text{ m}^{-2}$ (ρ_3), and $4.68 \times 10^9 \text{ m}^{-2}$ (ρ_4), respectively, using XRD. It is evident from Fig. 1(a) that dislocation density increases with surface roughness.

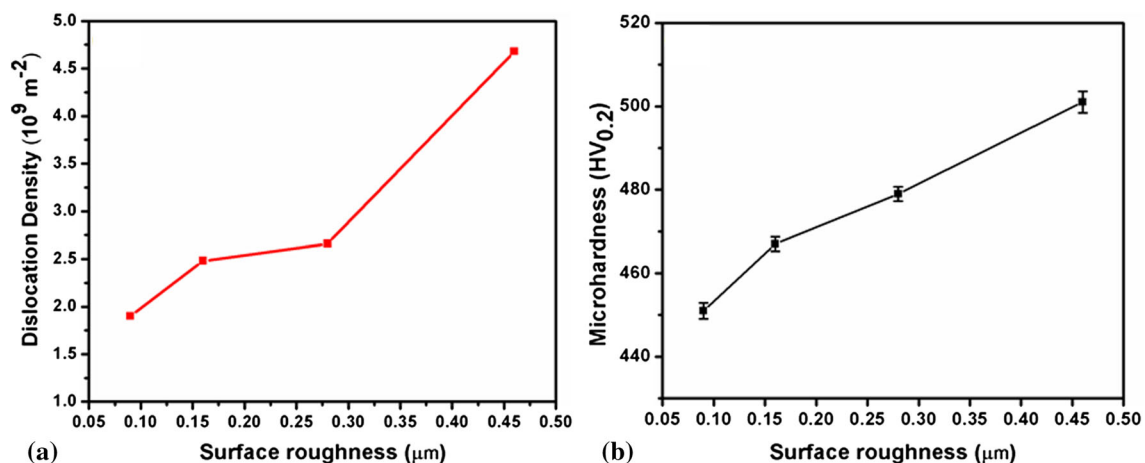


Fig. 1 Effect of surface roughness on: (a) dislocation density and (b) microhardness

Figure 1(b) shows variation of microhardness of the samples, ground with 1000 (R_{a1}), 800 (R_{a2}), 600 (R_{a3}), and 400 (R_{a4}) grit emery papers with R_a : 0.09, 0.16, 0.28, and 0.46 μm , respectively. Microhardness of the samples with surface roughness R_{a1} , R_{a2} , R_{a3} , and R_{a4} was 451 ± 1.9 , 466 ± 1.7 , 479 ± 1.7 , and 501 ± 2.7 HV, respectively. Thus, microhard-

ness of the samples gradually increased with increase in the surface roughness (Fig. 1b).

3.2 Grain Size Measurement of the Ultrasonic Shot Peened Samples

The grain refinement and microstructural phases were characterized using XRD analysis. Peaks of γ , γ' , and γ'' are shown in Fig. 2 for the un-shot peened and 5 min USPed samples. The matrix is γ , whereas γ' and γ'' are precipitate phases of $\text{Ni}_3(\text{Al, Ti})$ and Ni_3Nb with FCC and BCT crystal structure, respectively. No phase change was observed due to ultrasonic shot peening; however, there was peak broadening in the 5 min USPed sample in respect of the untreated one. The average grain size of the USPed samples was calculated using the Scherrer and Wilson equation (Ref 41).

$$D = \frac{0.9\lambda}{B \cos \theta} \quad (\text{Eq 2})$$

where λ is x-ray wavelength, θ is Bragg angle, and B is line broadening. The average grain size of the sample USPed for 5 min was found to be about 82 nm.

3.3 Hot Corrosion Kinetics

The influence of salt/salt mixtures on the hot corrosion behavior was established from the plots of square of weight gain per unit area with time of exposure. Negligible weight gain was found in the uncoated samples from exposure at 700 °C.

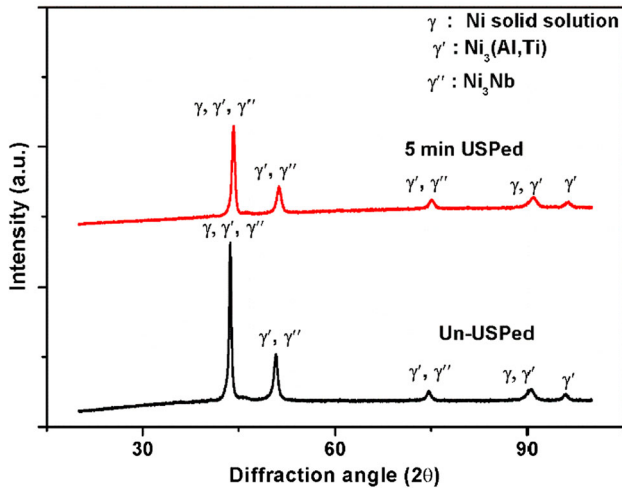


Fig. 2 X-ray diffraction of un-shot peened and ultrasonic shot peened superalloy IN718

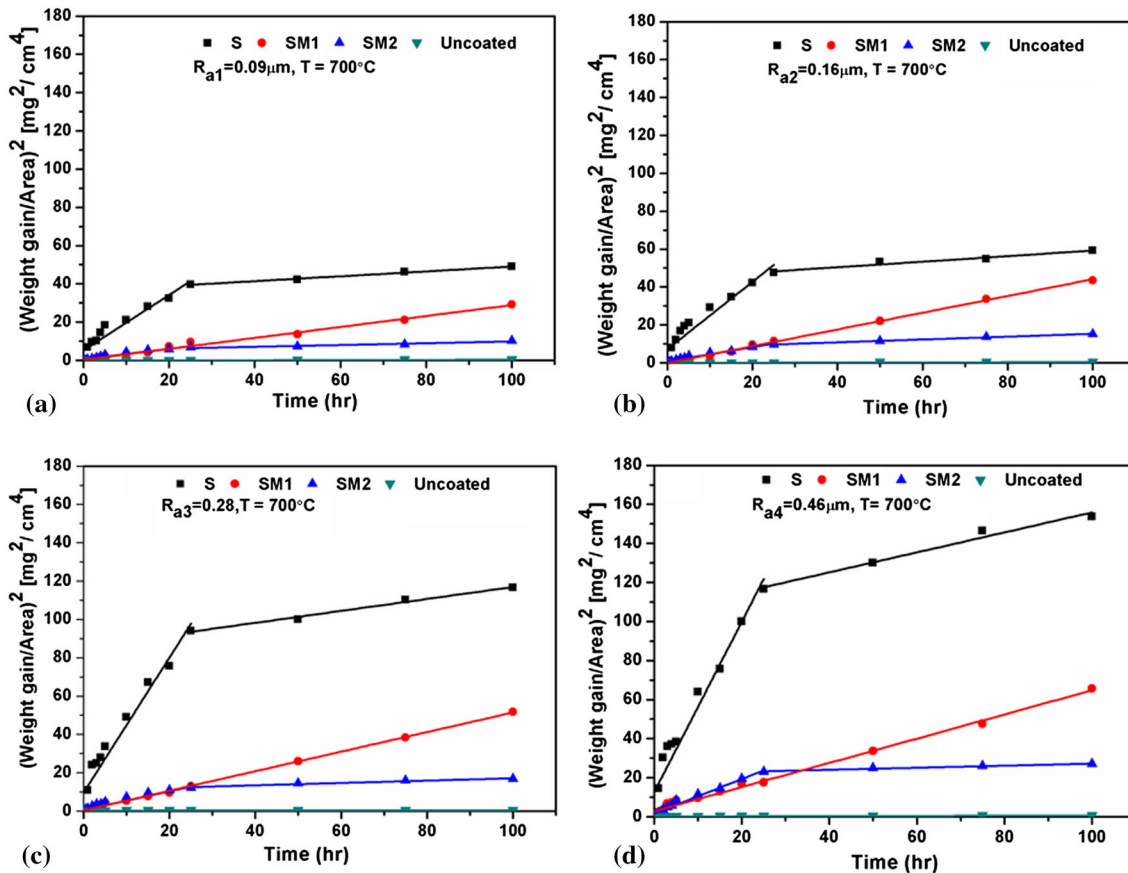


Fig. 3 Plots of square of weight gain per unit area vs. time from exposure at 700 °C for different surface roughness: (a) R_{a1} ; (b) R_{a2} ; (c) R_{a3} ; and (d) R_{a4} ; of the specimens coated with S, SM1, and SM2

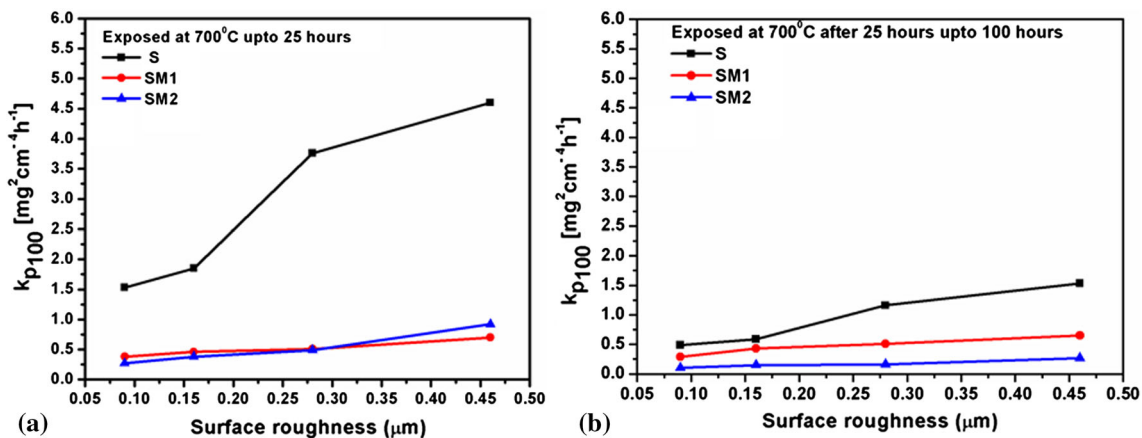


Fig. 4 Effect of surface irregularity on the parabolic rate constants of the samples coated with salt S and salt mixtures SM1 and SM2, exposed at 700 °C for different durations: (a) up to 25 h (b) from 25 to 100 h

However, significantly large weight gain was there in the samples coated with the salt S and the salt mixture SM1 as compared with that coated with the salt mixture SM2. The plots of the square of weight gain per unit area of the samples exposed at 700 °C for a period of 100 h are shown in Fig. 3. The samples coated with salt/salt mixture show parabolic behavior for the entire period of exposure of 100 h. The plot of the square of weight gain/area (mg^2/cm^4) versus time (hrs) is used to establish rate law for the process of hot corrosion. The parabolic rate constant k_p is calculated using equation $(\Delta W/A)^2 = k_p \times t + C$, where $\Delta W/A$ is weight gain per unit surface area (mg/cm^2), t is the time of exposure, and C is a constant (Ref 43).

The calculated values of the parabolic rate constants are shown in Fig. 4(a) and (b). A higher value of k_p implies faster rate of oxidation/corrosion at a given temperature. The value of k_p is found to be maximum for 700 °C in the sample coated with salt S. The weight gain plots are best fitted using linear least-square method. It is obvious from Fig. 4 that the value of k_p is higher for the sample exposed to salt S for all the different grades of roughness, than for those coated with the salt mixtures SM1 and SM2. Further, k_p increases with roughness of the surface in all the samples coated with S, SM1, and SM2. It is important to mention that at 600 °C the samples coated with SM1 showed lowest corrosion among the samples coated with salt S and the salt mixtures. On the other hand, the present study at higher temperature of 700 °C shows opposite behavior and the salt mixture SM1 is much more corrosive than the three salt mixture (SM2). Further, it is important to mention that at 700 °C the highest hot corrosion is from the coating of salt S, but the relative increase in the weight gain/area at 700 °C compared with that at 600 °C for the sample coated with salt S is only 49%, whereas it is 153% for the sample coated with salt mixture SM1, and only 8% for that coated with SM2. The effectiveness of ultrasonic shot peening on hot corrosion resistance is quite obvious from Table 1, showing weight gain per unit area for different roughness and the sample USPed for 5 min. Thus, it is obvious that there is increase in weight gain per unit area by 0.8, 2, 2.6, and 3.5 mg/cm^2 for the un-shot peened samples of varying roughnesses of R_{a1} , R_{a2} , R_{a3} , and R_{a4} , respectively, in respect of the sample with initial roughness 0.08 μm and subsequently subjected to USP for 5 min.

Table 1 Effect of ultrasonic shot peening and surface roughness on hot corrosion of the superalloy IN718 at 700 °C, exposed for 100 h

S. No.	Condition	Weight gain/area (mg/cm^2)
1	5 min USPed	4.6
2	Sample ground with 1000 (R_{a1})	5.4
3	Sample ground with 800 (R_{a2})	6.6
4	Samples ground with 600 (R_{a3})	7.2
5	Sample ground with 400 (R_{a4})	8.1

3.4 X-ray Diffraction Analysis

The nature of the phases formed from high-temperature corrosion affects the process of corrosion of the material. The XRD patterns of the un-shot peened and 5 min USPed samples coated with SM1 salt mixture after the exposure of 100 h at 700 °C are shown in Fig. 5. Several oxides, sulfides, vandates such as Cr_2O_3 , Fe_2O_3 , Fe_3O_4 , NiVO_3 , FeVO_4 , NaVO_3 , NiV_2O_7 , $\text{Ni}(\text{VO}_4)_7$, FeS , CrS , NiS , $\text{Na}_2\text{Cr}_2\text{O}_7$, NaCrO_4 , NiFe_2O_4 may be seen to form.

3.5 Diffusion of Corrosion Products

The samples hot corroded in the SM1 salt mixture, from the exposure of 100 h at 700 °C, were sectioned transversely, perpendicular to the corroded surface, to assess the depth of penetration of the corrodants below the surface, at different surface roughness and dislocation densities. Figure 6 shows that the depth of penetration of the corrosion products in the sample with different surface roughness is in the order: $R_{a4} > R_{a3} > R_{a2} > R_{a1}$, for the SM1 salt coated samples. Oxidation and sulfidation are found to be the main cause of damage for the SM1 coated samples.

3.6 Electron Probe Micro Analysis (EPMA)

Wavelength dispersive spectroscopy (WDS) was used for elemental mapping of the corroded samples. EPMA analysis of coated samples in the highest corrosive state (400 grit ground sample) and the sample USPed for 5 min was performed to examine the elemental distribution in these specimens. The

un-shot peened and shot peened samples corroded by SM1 coating, exposed at 700 °C for 100 h, were sectioned perpendicular to the corroded surface, and the elemental maps show variation of nickel, iron, chromium, oxygen in the hot corroded samples (Fig. 8). The diffusion of nickel, iron, and chromium from the base material toward the surface of the substrate resulted in formation of NiO, Fe₂O₃, Fe₃O₄, Cr₂O₃ oxides.

4. Discussion

There is little gain in the weight of the uncoated sample exposed at 700 °C, and small gain in the weight of the samples coated with the three salt mixture SM2, from exposure at 700 °C. This may be attributed to formation of an intact and protective oxide layer on the uncoated sample. On the other hand, there is significant gain in weights of the samples coated with the salt S, followed by that coated with the dual salt mixture SM1, from the exposure at 700 °C for 100 h. It may be seen that there are dual slopes in the plots of the square of weight gain per unit area versus the time of exposure in the samples coated with the salt S and the three salt mixture SM2 (Fig. 3). This behavior is attributed to spalling of scales in these samples due to the stresses induced by the oxide films during their growth. At some point, the increase in thickness of the scale is unable to sustain the associated stress and leads to breakage of the scale and subsequent spallation of the oxide layer (Ref 44). The partial spallation of scale in some regions exposes the subsurface of the alloy to air environment to cause oxidation at the exposed subsurface, and thus, the overall corrosion kinetics slows down. However, in the samples with coating of the salt mixture SM1, exposed at 700 °C for 100 h, the coating was found adherent and there was no spallation of scale; therefore, there is a single slope for this condition (Fig. 3).

In general, corrosion kinetics of the rough samples is found to be higher than those of the smoother ones. Also, the weight gain per unit area and k_p values are relatively higher for the samples exposed to salt S and the salt mixture SM1. Square of weight gain per unit area versus time plot show that corrosion rate is slow for the initial 5 h and increases rapidly till 25 h and remains almost constant up to 100 h, for the samples coated with salt S and the salt mixture SM2. The exposure of the first 25 h is more aggressive because of continuous formation of

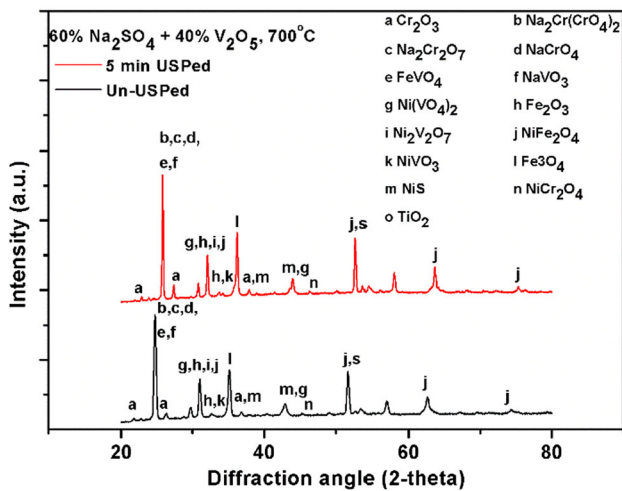


Fig. 5 X-ray diffraction patterns of the un-shot peened and 5 min ultrasonic shot peened samples coated with SM1 salt mixture and exposed at 700 °C up to 100 h

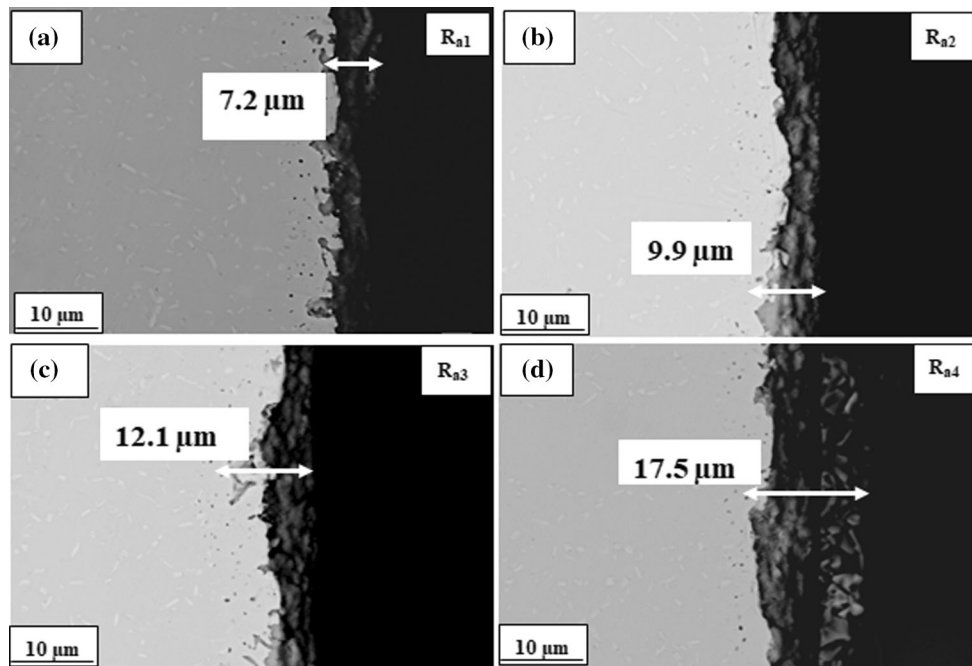


Fig. 6 SEM micrographs showing the effect of surface roughness on the depth of penetration of corrosion products in the samples coated with salt mixture SM1 and exposed at 700 °C for 100 h

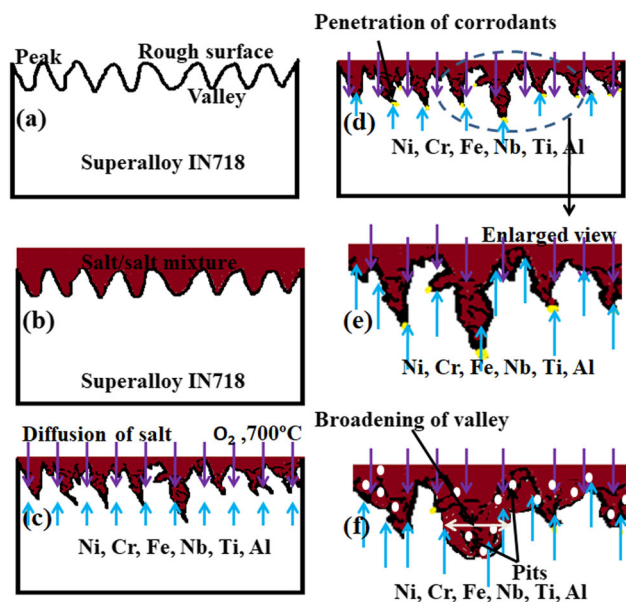


Fig. 7 Schematic showing the effect of surface roughness on hot corrosion of the superalloy IN718 at 700 °C

corrosion products over the substrate; however, the corrosion rate is slowed down after 25 h for the samples coated with salt S and the salt mixture SM2. The oxide layer was formed due to initial corrosion reaction and acted as a barrier against further penetration of the remaining salt/salt mixtures. On the other hand, samples coated with SM1 salt mixture show increasing trend of weight gain/area up to 100 h. Parabolic nature of hot corrosion is exhibited by all the samples coated with S, SM1, and SM2. The small deviation from the parabolic rate law could be due to cyclic scale growth. It may also be noticed that NaCl is most aggressive at 700 °C due to volatility of chlorides, and the SM2 salt mixture also shows aggressiveness at 700 °C due to sulfidation.

Mechanical grinding of surface causes cold deformation of the surface region, and the dislocation density increases (Fig. 1a). The dislocation density increases with surface roughness, likewise the microhardness also increases (Fig. 1b). The deleterious effect of cold working on corrosion resistance of the austenitic stainless steels was revealed in acidic and chloride containing media (Ref 45). In the case of a rougher surface, larger surface area is involved in the process of corrosion to result in high rate of corrosion (Ref 34, 46, 47). A schematic presentation of the probable mechanism of hot corrosion, based on the effect of surface roughness, is shown in Fig. 7. The ground surface exhibits various peaks and valleys at the surface of the sample (Fig. 7a). All the valleys get filled with deposition of salt/salt mixtures, whereas the peaks have much less amount of salt/salt mixtures for the reaction (Fig. 7b); therefore, the surfaces with deeper valleys undergo severe corrosion. Diffusion of salt/salt mixture starts at 700 °C toward interior of the specimen and diffusion of alloying elements toward the surface of specimen (Fig. 7c and d). Penetration of corrodants in the bulk of the specimen occurs through the valley (Fig. 7e). Figure 7(f) shows broadening of valley due to corrosive reactions taking place and the formation of oxides and pits at the interface of the alloy and corrodant.

The samples ground by the most rough emery paper (#400) with the average surface roughness $R_{a4} \approx 0.46 \mu\text{m}$ and the

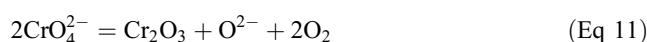
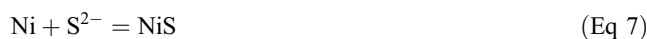
dislocation density $\rho_4 = 4.68 \times 10^9 \text{ m}^{-2}$, showed highest weight gain, and the most deleterious effect is observed in the samples coated with SM1, from exposure at 700 °C for 100 h. The depth of penetration of the corrosive species is found to be 7.2, 9.9, 12.1, and 17.5 μm corresponding to average roughness of R_{a1} , R_{a2} , R_{a3} , and R_{a4} from Fig. 6(a-d), respectively.

It was found that the severity of hot corrosion at 600 °C was in decreasing order from the coatings of salt S, followed by that of the salt mixture SM2 and was lowest in the salt mixture SM1. On the other hand, this sequence is changed as $S > \text{SM1} > \text{SM2}$ at 700 °C. Since the salt mixture SM1 undergoes eutectic melting at 603 °C (Ref 48), corrosion resistance of the sample coated with SM1 salt mixture at 600 °C was not much affected at 600 °C and the Cr_2O_3 layer formed was quite protective (Ref 49). The mechanism of hot corrosion of the sample coated with SM1, the most corrosive one with roughness R_{a4} and dislocation density, $\rho_4 = 4.68 \times 10^9 \text{ m}^{-2}$, was studied in detail.

Out of the four samples with different surface roughnesses exposed in the salt mixture SM1; the sample with the maximum surface roughness of R_{a1} showed much higher weight gain as compared with that exposed at 600 °C for 100 h. The surface with higher roughness was more susceptible to corrosive attack than the smoother ones due to its greater surface area. Oxygen penetrated the substrate and formed oxides of Cr, Fe, and Ni which led to weight gain. Some possible oxidation reactions with this salt mixture are reported in our earlier publication (Ref 34). The solubility of the protective oxides in the molten salt mixture SM1 is higher than that in Na_2SO_4 ; therefore, the dissolution of the protective oxide layer took place (Ref 50). V_2O_5 reacted with Cr_2O_3 , Fe_2O_3 , and NiO and formed vanadate compounds at the oxide salt interface along with the formation of $\text{Na}_2\text{Cr}_2\text{O}_7$. Dissociation of sodium sulfate to attain equilibrium at oxide/salt interface takes place. Basic fluxing process leads to formation of different products as per the following reactions (3-6):



Sulfur ions react with Cr, Fe, and Ni or with their oxides and form following sulfides which break the protective chromia layer (Ref 6).



The salt mixture SM1 with 60 wt.% Na_2SO_4 and 40 wt.% V_2O_5 forms a very hazardous and low melting phase of sodium meta vanadate (NaVO_3) with melting point of 610 °C (Ref 51) which significantly enhances the oxygen activity (Ref 50).

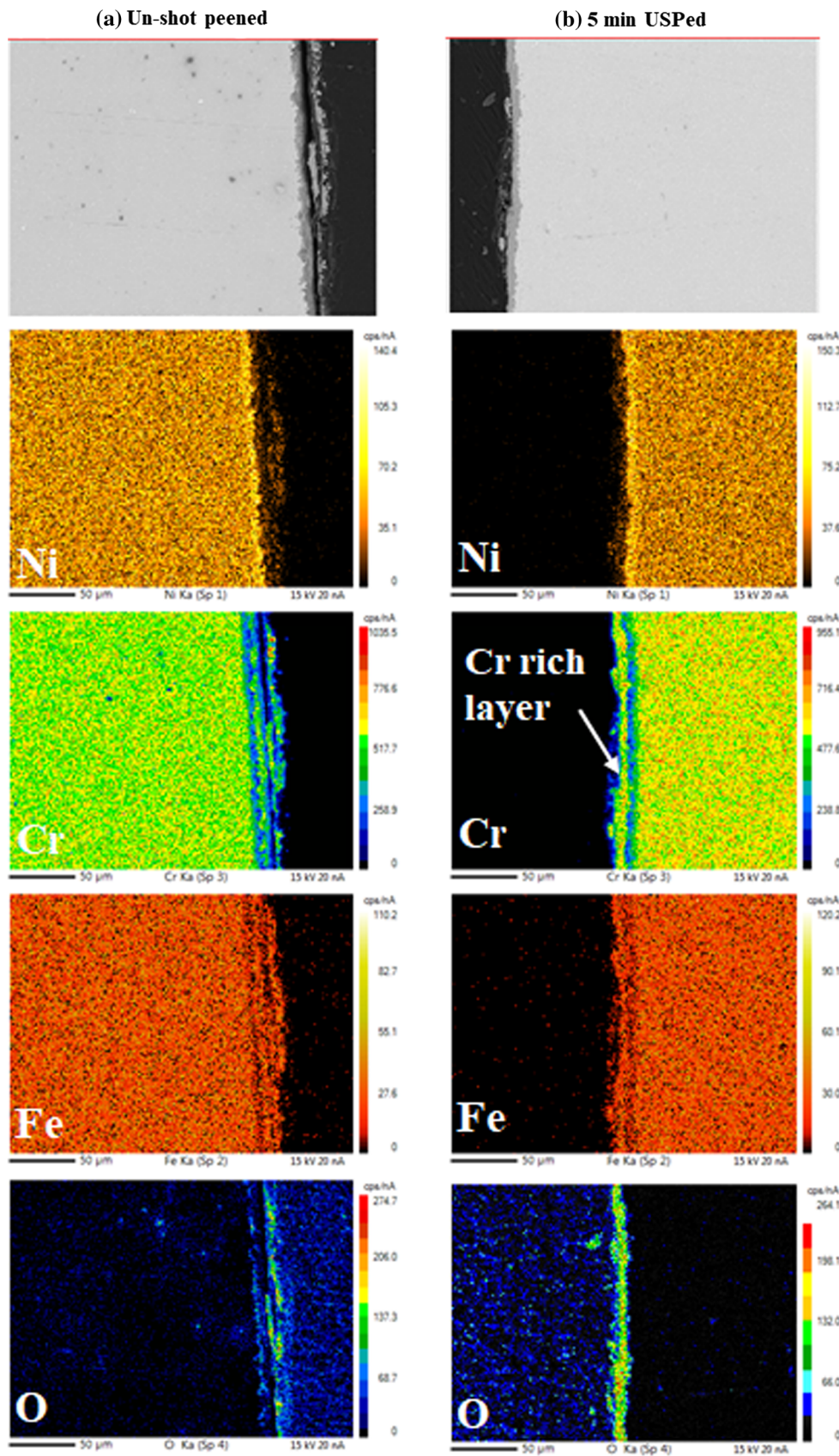
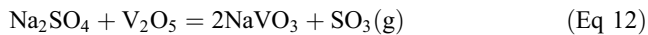


Fig. 8 EPMA/SE x-ray mapping of cross sections of specimens coated with salt mixture SM1 and exposed at 700 °C for 100 h, showing distribution of different elements: nickel, chromium, iron, and oxygen for (a) un-shot peened sample and (b) 5 min USPed sample



At 700 °C, the fluidity of the molten eutectic increases (Ref 49) and the increase in severity of hot corrosion led to weight gain per unit area of the SM1 coated samples. Vanadates are known to cause severe damage to protective oxide of Cr₂O₃ (Ref 50).

EPMA analysis also supports the above statement (Fig. 8a). Here, it is worth mentioning that the weight gain per unit area from the SM1 coating is nearly 153% more at 700 °C as compared with that at 600 °C (Ref 34). The EPMA results show the extent of diffusion of alloying elements from the substrate to surface and that of salt elements from the surface into the substrate. It may be seen that Cr was involved more in corrosion reaction during hot corrosion, as it is depleted more from the base alloy. The corrosion of the superalloy IN718 with the SM1 salt mixture coating, at 700 °C, is primarily by the oxidation process followed by sulfidation reactions as indicated above.

Furthermore, corrosion resistance is found to be enhanced by the novel process of ultrasonic shot peening. The presence of Cr₂O₃ layer on the shot peened samples resulted in improved corrosion resistance of the alloy because of extensive grain refinement at the surface. These results are in agreement with the earlier investigation (Ref 52). Here, the diffusivity of chromium increases with increase in the population of grain boundary which leads to formation of highly protective Cr₂O₃ as compared to that in the un-shot peened one (Ref 37). Oxygen diffusivity is increased on the modified surface before the formation of protective layer, and it is decreased after the formation of protective layer by covering the grain boundaries on the shot peened surface (Ref 39, 53). The more protective effect of the oxide layer of Cr₂O₃ formed at 700 °C on the USPed surface is quite evident from the much better uniformity and higher thickness of the compact Cr₂O₃ layer formed on the USPed sample (Fig. 8b).

5. Conclusions

The following conclusions are drawn from this study:

- (a) Hot corrosion of the superalloy IN718 coated with salt S and salt mixtures SM1 and SM2 exhibited parabolic kinetics at 700 °C. The weight gain analysis showed that IN718 had higher oxidation resistance at 700 °C without any coating and the salt S coated sample exhibited higher weight gain at 700 °C from exposure of 100 h as compared with the samples coated with the salt mixtures SM1 and SM2, in respect of that observed earlier at 600 °C.
- (b) The relative increase in weight gain/area from exposure at 700 °C as compared with that at 600 °C, from the salt S is only 49%, whereas it is 153% from SM1, and only 8% from the SM2 coating.
- (c) The solubility of the protective oxides in the molten salts of sulfate–vanadate mixture at 700 °C is higher than in Na₂SO₄; therefore, there was dissolution of the protective oxide layer.
- (d) The highly damaging low melting compound of NaVO₃ increased the severity of corrosion of the sample coated

- with SM1, enhancing the activity of oxygen.
- (e) Higher surface roughness increased the rate of corrosion due to nucleation and growth of oxides at the surface and penetration of corrosion products through the surface to the bulk of the alloy. Also, the sample with higher roughness had higher dislocation density and exhibited higher rate of corrosion.
- (f) Grain size of about 82 nm was produced by ultrasonic shot peening, it improved the hot corrosion resistance of the superalloy IN718 in the salt mixture SM1 at 700 °C, promoting formation of highly protective layer of Cr₂O₃.

Acknowledgments

The authors are thankful to Prof. N V C Rao and Dr. Dinesh Pandit, Department of Geology, Institute of Science, B.H.U., Varanasi for providing EPMA facility.

References

1. M. Sundararaman, P. Mukhopadhyay, and S. Banerjee, Precipitation of the δ-Ni₃Nb Phase in Two Nickel Base Superalloys, *Met. Trans A*, 1988, **19**(3), p 453–465
2. J.P. Collier, S.H. Wong, J.K. Tien, and J.C. Phillips, The Effect of Varying Al, Ti, and Nb Content on the Phase Stability of Inconel 718, *Met. Mater. Trans. A*, 1988, **19**(7), p 1657–1666
3. G.Y. Lai, *High-Temperature Corrosion and Materials Applications*, 1st ed., U.S.A. ASM International, 2007
4. N. Eliaz, G. Shemshand, and R.M. Latanision, Hot Corrosion in Gas Turbine Components, *Eng. Fail. Anal.*, 2002, **9**, p 31–43
5. G.S. Mahobia, N. Paulose, S.L. Mannan, R.G. Sudhakar, K. Chattopadhyay, N.C.S. Srinivas, and V. Singh, Effect of Hot Corrosion on Low Cycle Fatigue Behavior of Superalloy IN718, *Int. J. Fatigue*, 2014, **59**, p 272–281
6. V. Mannava, A.S. Rao, N. Paulose, M. Kamaraj, and R.S. Kottada, Hot Corrosion Studies on Ni-Base Superalloy at 650 °C Under Marine-Like Environment Conditions Using Three Salt Mixture (Na₂SO₄ + NaCl + NaVO₃), *Corr. Sci.*, 2016, **105**, p 109–119
7. F. Mansfeld, N.E. Paton, and W.M. Robertson, The High Temperature Behavior of Superalloys Exposed to Sodium Chloride: II, Corrosion, *Met. Mater. Trans. B*, 1973, **4**(1), p 321–327
8. F. Saegusa and D.A. Shores, Corrosion Resistance of Superalloys in the range 800–1300 F (430–700 °C), *J. Mater. Energy Syst.*, 1982, **4**(1), p 16–27
9. K.A. Ellison, P. Lowden, J. Liburdi, and D.H. Boone, *Repair joints in nickel-based superalloys with improved hot corrosion resistance*, International Gas Turbine and Aeroengine Congress and Exposition, Cincinnati, 1993, p 24–27
10. L. Jian, C.Y. Yuh, and M. Farooque, Oxidation Behavior of Superalloys in Oxidizing and Reducing Environments, *Corr. Sci.*, 2000, **42**(9), p 1573–1585
11. S. Prakash, D. Puri, and H. Singh, Hot Corrosion Behaviour of Plasma Sprayed Coatings on a Ni-Based Superalloy in Na₂SO₄-60% V₂O₅ Environment, *ISIJ Int.*, 2005, **45**(6), p 886–895
12. T.S. Sidhu, S. Prakash, and R.D. Agrawal, Characterisations of HVOF Sprayed NiCrBSi Coatings on Ni- and Fe-Based Superalloys and Evaluation of Cyclic Oxidation Behaviour of Some Ni-Based Superalloys in Molten Salt Environment, *Thin Solid Films*, 2006, **515**(1), p 95–105
13. T.S. Sidhu, S. Prakash, and R.D. Agrawal, Study of Molten Salt Corrosion of High Velocity Oxy-Fuel Sprayed Cermet and Nickel-Based Coatings at 900 °C, *Met. Mater. Trans. A*, 2007, **38**(1), p 77–85
14. S.H. Cho, I.J. Cho, G.S. You, J.S. Yoon, and S.W. Park, Corrosion Behavior of Ni-Base Alloys in a Hot Lithium Molten Salt Under an Oxidizing Atmosphere, *MMI*, 2007, **13**(4), p 303–309
15. S. Kamal, R. Jayaganthan, S. Prakash, and S. Kumar, Hot Corrosion Behavior of Detonation Gun Sprayed Cr₃C₂-NiCr Coatings on Ni and

- Fe-Based Superalloys in Na₂SO₄-60% V₂O₅ Environment at 900 °C, *J. Alloys Compd.*, 2008, **463**(1), p 358–372
16. L. Xueming, S. Wenru, G. Shouren, and H. Zhuangqi, Hot Corrosion Behavior of IN718 Alloy and Its Effect on Mechanical Properties, *Rare Met. Mater. Eng.*, 2008, **2**, p 016
 17. G. Sreedhar, M.D.M. Alam, and V.S. Raja, Hot Corrosion Behaviour of Plasma Sprayed YSZ/Al₂O₃ Dispersed NiCrAlY Coatings on Inconel-718 Superalloy, *Surf. Coat. Tech.*, 2009, **204**(3), p 291–299
 18. G. Sreedhar and V.S. Raja, Hot Corrosion of YSZ/Al₂O₃ Dispersed NiCrAlY Plasma-Sprayed Coatings in Na₂SO₄-10 wt.% NaCl Melt, *Corr. Sci.*, 2010, **52**(8), p 2592–2602
 19. S. Kamal, R. Jayaganthan, and S. Prakash, High Temperature Cyclic Oxidation and Hot Corrosion Behaviours of Superalloys at 900 °C, *Bull. Mater. Sci.*, 2010, **33**(3), p 299–306
 20. J.L. Trinstancho-Reyes, M. Sanchez-Carrillo, R. Sandoval-Jabalera, V.M. Orozco-Carmona, F. Almeraya-Calderon, J.G. Chacon-Nava, J.G. Gonzalez-Rodriguez, and A. Martinez-Villafane, Electrochemical Impedance Spectroscopy Investigation of Alloy Inconel-718 in Molten Salts at High Temperature, *Int. J. Electrochem. Sci.*, 2011, **6**, p 419–431
 21. A. Rahman, V. Chawla, R. Jayaganthan, R. Chandra, and R. Ambardar, Study of Cyclic Hot Corrosion of Nanostructured Cr/Co-Al Coatings on Superalloy, *Mater. Chem. Phys.*, 2011, **126**(1), p 253–261
 22. W. Garkas, S. Weiß, and Q.M. Wang (Cr_{1-x}Al_x)N as a Candidate for Corrosion Protection in High Temperature Segments of CCS Plants, *Environ. Earth Sci.*, 2013, **70**(8), p 3761–3770
 23. S. Saladi, J. Menghani, and S. Prakash, Hot Corrosion Behaviour of Detonation-Gun Sprayed Cr₃C₂-NiCr Coating on Inconel-718 in Molten Salt Environment at 900 °C, *Trans. IIM*, 2014, **67**(5), p 623–627
 24. A. Ajay, V.S. Raja, G. Sivakumar, and S.V. Joshi, Hot Corrosion Behavior of Solution Precursor and Atmospheric Plasma Sprayed Thermal Barrier Coatings, *Corr. Sci.*, 2015, **98**, p 271–279
 25. C.J. Wang and Y.C. Chang, NaCl-Induced Hot Corrosion of Fe-Mn-Al-C Alloys, *Mater. Chem. Phys.*, 2002, **76**(2), p 151–161
 26. T.S. Sidhu, A. Malik, S. Prakash, and R.D. Agrawal, Cyclic Oxidation Behavior of Ni-and Fe-Based Superalloys in Air and Na₂SO₄-25% NaCl Molten Salt Environment at 800 °C, *Int. J. Phys. Sci.*, 2006, **1**(1), p 027–033
 27. H. Singh, D. Puri, and S. Prakash, An Overview of Na₂SO₄ and/or V₂O₅ Induced Hot Corrosion of Fe-and Ni-Based Superalloys, *Rev. Adv. Mater. Sci.*, 2007, **16**(1), p 27–50
 28. R.A. Rapp, Hot Corrosion of Materials: A Fluxing Mechanism, *Corr. Sci.*, 2002, **44**(2), p 209–221
 29. J.R. Nicholls, Designing Oxidation-Resistant Coatings, *JOM*, 2000, **52**(1), p 28–35
 30. M.Y. Nazmy, The Effect of Environment on the High Temperature Low Cycle Fatigue Behaviour of Cast Nickel-Base IN-738 Alloy, *Mater. Sci. Eng.*, 1982, **55**(2), p 231–237
 31. M.Y. Nazmy, Effect of Room Temperature Prestrain and Subsequent Heat Treatment on the Creep Life of a Ni-Base Superalloy, *Scripta Met.*, 1982, **16**(12), p 1329–1332
 32. M. Yoshida, Effect of Hot Corrosion on the Mechanical Performances of Superalloys and Coating Systems, *Corr. Sci.*, 1993, **35**(5), p 1115–1124
 33. R. Walter and M.B. Kannan, Influence of Surface Roughness on the Corrosion Behaviour of Magnesium Alloy, *Mater. Des.*, 2011, **32**(4), p 2350–2354
 34. D. Pradhan, G.S. Mahobia, K. Chattopadhyay, and V. Singh, Effect of Surface Roughness on Corrosion Behavior of the Superalloy IN718 in Simulated Marine Environment, *J Alloys Compd.*, 2018, **740**, p 272–281
 35. S. Kumar, G.S. Rao, K. Chattopadhyay, G.S. Mahobia, N.S. Srinivas, and V. Singh, Effect of Surface Nanostructure on Tensile Behavior of Superalloy IN718, *Mater. Des.*, 2014, **62**, p 76–82
 36. A. Sanda, V. Garcia Navas, and O. Gonzalo, Surface State of Inconel 718 Ultrasonic Shot Peened: Effect of Processing Time, Material and Quantity of Shot Balls and Distance from Radiating Surface to Sample, *Mater. Des.*, 2011, **32**(4), p 2213–2220
 37. L. Tan, X. Ren, K. Sridharan, and T.R. Allen, Effect of Shot-Peening on the Oxidation of Alloy 800H Exposed to Supercritical Water and Cyclic Oxidation, *Corr. Sci.*, 2008, **50**, p 2040–2046
 38. X.Y. Zhang, M.H. Shi, C. Li, N.F. Liu, and Y.M. Wei, The Influence of Grain Size on the Corrosion Resistance of Nanocrystalline Zirconium Metal, *Mater. Sci. Eng., A*, 2007, **448**, p 259–263
 39. S. Kumar, K. Chattopadhyay, G.S. Mahobia, and V. Singh, Hot Corrosion Behaviour of Ti-6Al-4V Modified by Ultrasonic Shot Peening, *Mater. Des.*, 2016, **110**, p 196–206
 40. G. Dini, R. Ueji, and A. Najafzadeh, Flow Stress Analysis of TWIP Steel Via the XRD Measurement of Dislocation Density, *Mater. Sci.*, 2010, **527**, p 2759–2763
 41. J.I. Langford and A.J.C. Wilson, Scherrer After Sixty Years: A Survey and Some New Results in the Determination of Crystallite Size, *J. App. Cryst.*, 1978, **11**(2), p 102–113
 42. G. Williamson and W. Hall, X-ray Line Broadening from Filled Aluminium and Wolfram, *Acta Metall.*, 1953, **1**, p 22–31
 43. N.B. Pilling and R.E. Bedworth, The Oxidation of Metals at High Temperatures, *J. Inst. Met.*, 1923, **29**, p 529–591
 44. A.S. Khanna, *Introduction to High Temperature Oxidation and Corrosion*, ASM International, Russell Township, 2002
 45. W. Ozgovicz, A. Kurc-Lisiecka, and A. Grajcar, *Corrosion Behaviour of Cold-Deformed Austenitic Alloys, Environmental and Industrial Corrosion-Practical and Theoretical Aspects*, InTech, London, 2012
 46. S.J. Balsone, *The Effect of Stress and Hot Corrosion on Nickel-Base Superalloys*, Air Force Institute of Technology, Wright-Patterson Air Force Base, 1985
 47. P.S. Sidky and M.G. Hocking, The Hot Corrosion of Ni-Based Ternary Alloys and Superalloys for Application in Gas Turbines Employing Residual Fuels, *Corr. Sci.*, 1987, **27**(5), p 499–530
 48. E. Otero, M.C. Merino, A. Pardo, M.V. Biezma, and G. Buitrago, Study on Corrosion Products of IN657 Alloy in Molten Salts, *Key Eng. Mater.*, 1987, **20**(4), p 3583–3591
 49. C. Cuevas-Arteaga, Corrosion Study of HK-40 m Alloy Exposed to Molten Sulfate/Vanadate Mixtures Using the Electrochemical Noise Technique, *Corr. Sci.*, 2008, **50**, p 650–663
 50. J. Porcayo-Calderon, V.M. Salinas Bravo, R.A. Rodriguez-Diaz, and L. Martinez-Gomez, Effect of the NaVO₃-V₂O₅ Ratio on the High Temperature Corrosion of Chromium, *Int. J. Electrochem. Sci.*, 2015, **10**, p 4928–4945
 51. M.S. Doolabi, B. Ghasemi, S.K. Sadmezhaad, A. Habibollahzadeh, and K. Jafarzadeh, Hot Corrosion Behavior and Near-Surface Microstructure of a Low-Temperature High-Activity Cr-Aluminide Coating on Inconel 738LC Exposed to Na₂SO₄, Na₂SO₄ + V₂O₅ and Na₂SO₄ + V₂O₅ + NaCl at 900 °C, *Corr. Sci.*, 2017, **128**, p 42–53
 52. H. Matsuo, Y. Nishiyama, and Y. Yamadera, Steam oxidation properties of fine grain steels, in: *Proceedings from the Fourth International Conference on Advances in Materials Technology of Fossil Power Plants*, Hilton Head Island, South Carolina, 25–28 October 2004
 53. Z.B. Wang, N.R. Tao, W.P. Tong, J. Lu, and K. Lu, Diffusion of Chromium in Nanocrystalline Iron Produced by Means of Surface Mechanical Attrition Treatment, *Acta Mater.*, 2003, **51**, p 4319–4329